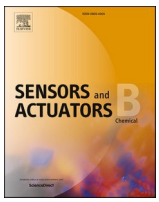
Sensors & Actuators: B. Chemical 359 (2022) 131584



Contents lists available at ScienceDirect

Sensors and Actuators: B. Chemical

journal homepage: www.elsevier.com/locate/snb





Alkali hydrolysis and Lewis acids assisted enhancement based highly sensitive and quantitative detection of malathion in tea using SERS and multivariate analysis

Xiaojing Chen, Xixi Huang, Shiliang Chen *, Shujat Ali, Xi Chen, Leiming Yuan, Wen Shi, Guangzao Huang

College of Electrical and Electronic Engineering, Wenzhou University, Wenzhou 325035, PR China

ARTICLE INFO

Keywords:
Hydrolysis
Malathion
Organophosphorus pesticide
Surface enhanced Raman scatting (SERS)
Rapid detection
Multivariate analysis

ABSTRACT

This study establishes an incredibly simple method for trace detection of malathion (MLT) by using spherical Ag nanoparticles (Ag NPs) based on surface enhanced Raman scatting (SERS). MLT was rapidly hydrolyzed through β-elimination reaction under alkaline condition, then provided a favorable ionic environment for SERS detection by using Lewis acids (LAs), leading to a 305 times maximum additional enhancement, and a limit of detection (LOD) as low as 0.1 ppb was achieved. The different alkaline hydrolysis pathways of MLT and other dithiophosphate organophosphorus molecules was clarified, and the conversion of molecular binding states on nanosurface were determined. The method was successfully applied in various tea samples, a LOD as low as 0.05 ppm was obtained. Due to the complex variation of characteristic peaks intensity, multivariate analysis method was used for quantitative analysis and a high determination coefficient (R^2 =0.9573) and good dynamic range of 0.1–5 ppm were obtained.

1. Introduction

Malathion (1, 2-bis (ethoxy carbonyl) ethyl O, O-dimethyl phosphorodithioate, MLT) is an organophosphorus pesticide that extensively used in agriculture to protect fruits, vegetables, tobacco and tea [1]. Overuse of MLT and other similar pesticides during the planting season or in post-harvest handling may result in excessive residue which can cause serious hazards to the environment and food safety [2]. Therefore, it is important to detect MLT residue in agricultural products.

Various traditional analysis methods have been successfully employed for organophosphorus pesticides detection [3–6], including gas chromatography (GC) coupled with mass spectrometry (GC-MS), high performance liquid chromatography (HPLC)coupled with mass spectrometry (LC-MS) [7–9]. However, these methods have disadvantages of complicated preparation, time consuming, expensive equipment and requires professional operators. Thus, to overcome these drawbacks, we propose a novel approach to rapidly detect MLT in tea using surface-enhanced Raman scattering (SERS), which can provide an ultra-sensitive "fingerprint" Raman information [5,6,10,11]. Here, molecular detection method, pre-treatment assay and quantitative model were systematically combined to overcome the problem of sensitive, rapid and quantitative detection of MLT in complex practical system.

Previously, several SERS-based sensors with different strategies for MLT detection have been reported. For instance, Yazdi et al. have reported the optofluidic SERS device which detected MLT in water up to a concentration of 12 ppb using a nanoporous microfluidic matrix [12]. Yu et al. have developed a new SERS-based sensor called Ag-NP-loaded filter membrane which obtained a detection limit of 61.5 ppb [13]. Similarly, a paper dipstick or swab-based approach have been adopted with lateral flow and SERS assays on an inkjet-printed plasmonic substrate and achieved a detection limit as low as 413 pg/5 μL (82.6 ppb) for MLT [14]. Nie et al. have used an aptamer-based SERS sensor for MLT detection, which presented a good linear range of 0.5–10 μM [15]. Despite the many innovations and improvements of materials and methods, the LODs of the above approaches for pure MLT detection were hardly down to 10 ppb, which make it difficult for further application studies under complex matrix interference. Furthermore, Fathi et al. have used electrochemistry combined with SERS and investigated the interaction of silver nanostructure modified electrode with MLT hydrolysates, which obtained a LOD of 10 pM for MLT [16]. However, each

* Corresponding author.
E-mail addresses: chenxj@wzu.edu.cn (X. Chen), Chenshiliang20@163.com (S. Chen).

https://doi.org/10.1016/j.snb.2022.131584
Received 20 November 2021; Received in revised form 7 February 2022; Accepted 14 February 2022
Available online 16 February 2022
0925-4005/© 2022 Elsevier B.V. All rights reserved.

test of the study requires to prepare the silver nanostructure from the precursor materials on the surface of the electrode and hydrolyze the MLT under the strong alkaline solution condition, which made it impossible to perform a simple and rapid detection. Hence, there is an urgent need to develop a SERS-based approach for practical detection of MLT which has been ignored in previous studies.

To meet the urgent need for practicable SERS-based analysis in complex matrix, we developed a simple and efficient detection method for trace analysis of MLT based on the strategy of rapid hydrolysis of MLT through β-elimination reaction in a dilute alkali environment (0.1 M NaOH). Then, Lewis acid (LA) was utilized to create a proton-rich or complexation environment which improved the competing advantage and controlled the binding states of target hydrolysate on the nano-surface. Significantly, the complexation of the target hydrolysate with NH_3 (formed by NH_4^+) resulted in approximately 305 times of additional enhancement compared with none LA addition group. Thus, trace detection was achieved on the simplest SERS substrate (spherical Ag NPs). The primary advantages of the method are no complicated SERS-material fabrication and operation steps nor other technical assistance, the whole detection process can be completed in 1 min and practically applicable for real sample analysis. In addition, the alkali hydrolysis pathway of MLT was studied through SERS and GC-MS. It was found that dimethyl dithiophosphate (DMDTP) was generated through β-elimination reaction, instead of dimethyl thiophosphate (DMTP) through nucleophilic substitution (S_N2) reaction which was considered in many studies [16–18]. The new and prominent SERS signal obtained in this study was completely different from all previous studies. By analyzing the signal, the pathways of binding model conversion of target hydrolysate on the nanoparticles surface and the mechanism of SERS signal change were revealed in detail. These analyses will provide a broad and valuable reference for future research on other similar molecules.

Furthermore, different from the above-mentioned studies which detected MLT just in water, our approach has been applied in various kinds of tea which contain lots of matrices, such as tea polyphenol, theophylline, amino acids and lipids etc [19–23], considered as an enormous challenge for qualitative and quantitative detection. The pre-treatment operation method just includes three simple steps and the whole process can be completed in 5 min, the resulting LOD was only one-tenth of the MRL (0.5 ppm) required by China, Japan and the European Union. For improving the feasibility of quantitative analysis, multivariate analysis (MVA) was employed [24], which can solve the problem of characteristic variable change and improve the accuracy and stability of the model compared with univariate analysis (UVA).

This work was committed to develop an operational, rapid and economical approach for the detection of MLT in tea, without peculiar SERS substrates and complex pretreatment process. Ultimately, solved the systematic engineering problem which was oscillating between high sensitivity in detection and low feasibility in application. Consequently, the method possesses a great application potential and can be extended to other SERS-materials and real objects analysis.

2. Experimental methods

2.1. Materials and chemicals

Malathion (99.8%) was purchased from Sinopharm Chemical Reagent Co., Ltd. (Beijing, China). Silver nitrate ($AgNO_3$, 99.8%), graphitized carbon black (GCB, 120–400 mesh), octadecyl silica (C18, 50 μm) and primary secondary amine (PSA, 50 μm) were bought from ANPEL Laboratory Technologies (Shanghai) Inc. Trisodium citrate dihydrate (99%), sulfuric acid (AR), hydrochloric acid (AR), acetonitrile (GR), acetone (GR), ammonium chloride (99%), calcium chloride (99%), aluminum chloride (PT), potassium iodide (≥99%), potassium bromide (99%), potassium chloride (99%), sodium chloride (99%), sodium sulfate (99%), sodium dihydrogen phosphate (≥99%), sodium bicarbonate (AR), sodium hydroxide (99%), zinc sulfate (99%), copper sulfate (99%) and anhydrous magnesium sulfate (99%) were purchased from Macklin Biochemical Technology Co., Ltd. (Shanghai, China). Thioglycolic acid (TGA, 99%), L-cysteine (99%), and cysteamine (98%) were obtained from B&K reagent Co., Ltd. (Beijing, China). DMDTP (97%) was purchased from Qingdao Tenglong Microwave Technology Co., Ltd (Qingdao, China). DMTP (98%) was purchased from Beijing VsciChem Technology Co., Ltd (Beijing, China). Tea samples were obtained from different sources, as detailed in Supporting information.

2.2. Preparation of spherical Ag nanoparticles

The Ag nanoparticles were prepared by the sodium citrate reduction method. In brief, 0.5 mL of trisodium citrate dihydrate solution (1% wt) was added to 49.5 mL of a boiling $AgNO_3$ aqueous solution (0.01 M) (glycerin bath) and stirred for 20 min. Then, 0.7 mL of trisodium citrate dihydrate (1% wt) was added and stirred for 15 min. The reaction mixture was cooled to room temperature, yielded an earthy-yellow Ag colloid.

2.3. Characterization methods

Transmission electron microscope (TEM) (JEM-2100 F, Shimadzu Co., Japan) was used to characterize the shape and size of Ag NPs. A droplet (5 μL) of Ag colloid was dropped onto the surface of copper grid (carbon-coated), dried, and then examined by the TEM system operated at 200 KV. Nano Measurer 1.2 program was applied to measure the particle size distribution by using 64 well-defined Ag NPs (Fig. S1).

Ultraviolet and visible spectrophotometer (UV–vis 2450, Shimadzu Co., Japan) was used to observe the extinction spectra. The Ag colloid was diluted 3 times for analysis.

Fourier Transform Infrared Spectroscopy (FTIR, Bruker VERTEX 70, Germany) was used to confirmed the organic groups of Ag NPs surface, with a resolution of 4 cm^{-1} and scan range of 4000–600 cm^{-1}. The Ag NPs sample was centrifugally concentrated (100 times) to remove the dissociative sodium citrate from the solution and then dropped onto the diamond surface of the ATR module for detection.

X-ray diffractometer (XRD) (D8 advance powder X-ray diffractometer, Bruker AXS, Germany) was used to examine the nature (crystallographic form) of the Ag NPs. The Ag colloid was concentrated one hundred times, dropped on a silicon wafer substrate, dried, and then repeated the above steps three times, finally examined by the XRD system. The applied operating voltage and current parameters were 40 kV and 40 mA, the graphite mono-chromatized was Cu-Kα1 radiation ($\lambda = 1.54184$ Å). The diffraction angle (2θ) was varied from 10° to 80° at a scanning rate of 0.05°/s.

Inductively coupled plasma mass spectrometry (ICP-MS, Agilent 7700, US) was used for the Ag concentration determination. For the sample preparation, 1 mL of Ag colloid was concentrated 100 times via centrifugation to remove the Ag^+, and then dissolved in 1 mL of concentrated HNO_3. The resultant solution was further diluted 100 times for ICP-MS analysis.

Gas chromatography-mass spectrometry (GC-MS) (7890A-5975 C, with triple-axis detector, Agilent Technologies, US) was used to identify the components of MLT alkaline hydrolysates. The aqueous alkaline hydrolysates were dissolved in acetonitrile (1:1, volume) and layered with excess sodium chloride solids, and then the acetonitrile layer was dehydrated with anhydrous sodium sulfate for further GC-MS analysis.

2.4. Methods for pre-treatment of tea and detection

For the pre-treatment, 0.2 g of tea (ground into powder or particles) was taken in a centrifugal tube, added 1 mL of acetonitrile and 0.1 g of anhydrous sodium sulfate if the tea sample was damp (such as fresh tea leaves). The sample was ultrasonically extracted for 3 min, 0.5 mL of the supernatant was taken and added into another centrifugal tube containing 10 mg GCB, and centrifuged for 10 s after mixing. The obtained

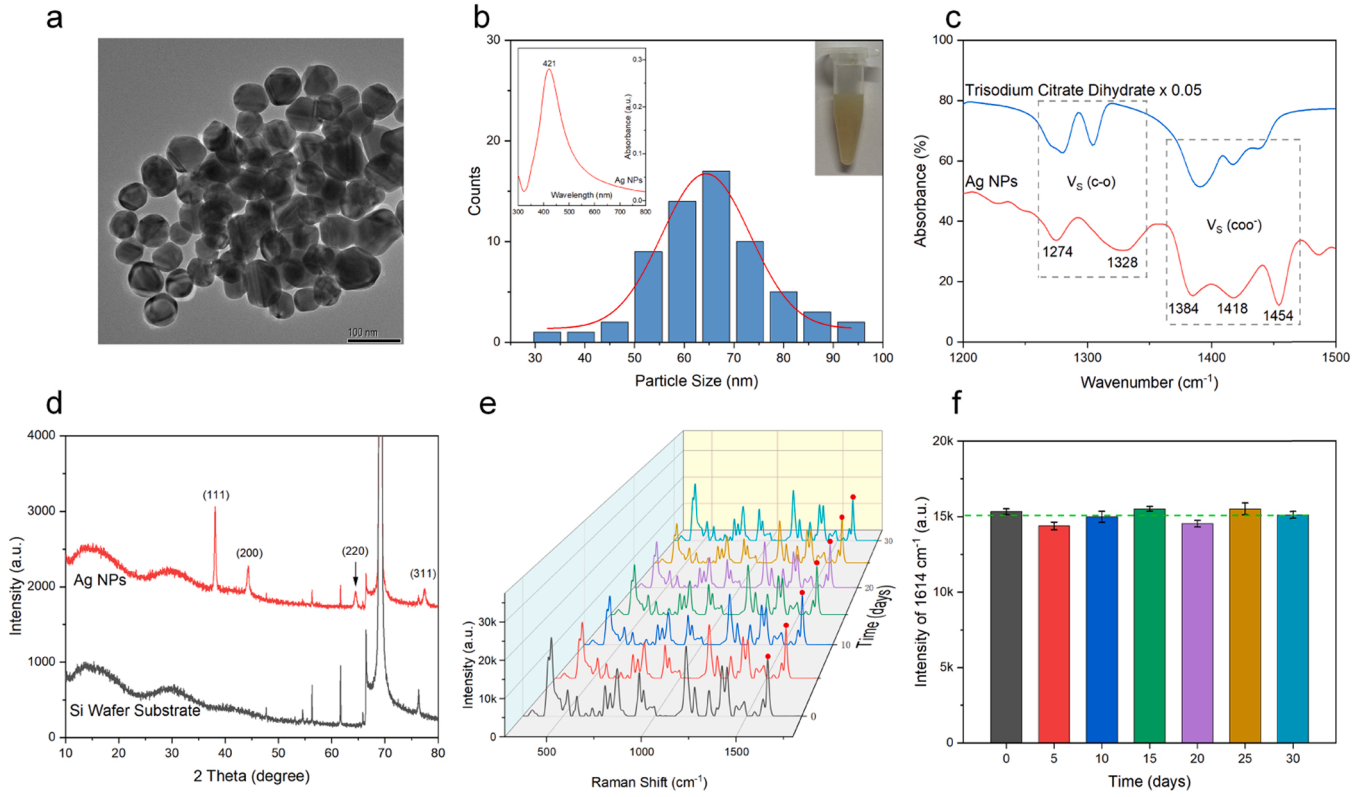


Fig. 1. TEM image (a) and the nanoparticles size distribution (b) of Ag NPs, the insets are the image of Ag NPs and corresponding UV–vis spectra. (c) FTIR spectra of trisodium citrate dihydrate and Ag NPs at 1500–1200 cm^{-1}, the dotted frames indicate the homogeneous molecular vibrations. (d) XRD pattern of Ag NPs on Si wafer substrate. (e) Raman spectra of freshly prepared Ag colloid to MG at different storage stages (0–30 days) and (f) corresponding signal intensity (1614 cm^{-1}). The error bars represent the standard deviation (n = 3). The dotted green line represents the average intensity. The test conditions were 200 μL MG sample (10 ppb), 50 μL Ag colloid, and 50 μL potassium iodide (0.5 M) as aggregator, mixed in turn and detected by 785 nm Raman spectrometer (500 mw, 1 s).

supernatant was used for SERS detection.

For detection, 40 μL of the above supernatant and 160 μL of ultrapure water were added into a glass detection cell. Then, 20 μL of 1 M sodium hydroxide was added, mixed and immediately added 20 μL of 1 M ammonium chloride. Subsequently, 50 μL of Ag NPs were added, mixed and detected under 785 nm Raman spectrometer (ATR3110, Optosky Co., Xiamen). All the above steps were performed without any specific and additional reserved incubation time.

For standard sample analysis, 20 μL of 1 M of sodium hydroxide was added to 200 μL of standard MLT sample in a glass detection cell, mixed, and then X μL of Y M of LA was added immediately. For the optimal condition, the volume and concentration parameters of different LAs (X, Y) were HCl (40, 1), H_2SO_4 (60, 0.5), $CaCl_2$ (40, 0.5), NaH_2PO_4 (40, 0.5), $AlCl_3$ (40, 0.33) and NH_4Cl (20, 1). Finally, 50 μL Ag NPs were added, mixed and incubated for 2 min, and detected by a 785 nm Raman spectrometer.

2.5. Density functional theory (DFT) calculations

DFT was used to optimize the structures of MLT and DMDTP via Gaussian 09 program based on the B3LYP functional [25,26] and 6–31 +G(d) basis sets. The VEDA4 program [27] was used to perform normal-mode analysis. The Multiwfn [28] and VMD program were used to map the molecular electrostatic potential (MEP). The MEP of MLT was calculated, and the molecular orbit and simulation Raman spectrum of DMDTP were analyzed.

2.6. Algorithms for quantitative analysis

Univariate and multivariate analysis methods were used for quantitative analysis. According to the relationship between unitary SERS characteristic peak intensity and MLT concentrations added in tea samples, a univariate linear regression (ULR) model was established as the following equation:

$$Y = \beta X + \varepsilon \quad (1)$$

Here, Y is the predicted value of the sample, represents the dependent variable in the regression model. X is the characteristic value of the sample, represents the independent variable in the regression model. β is the coefficient matrix. ε is the error term in the regression model. In multivariate modeling method, the relationship between the intensity of multiple SERS characteristic peaks and MLT concentration added in tea samples was comprehensively considered, and a multivariate linear regression (MLR) model was established as the following equation:

$$Y_{m\times k} = X_{m\times n}\beta_{n\times k} + \in_{m\times k} \quad (2)$$

Here, $X_{m\times n}$ is a matrix of m samples and n peak variables, $Y_{m\times k}$ is a matrix of m samples and k concentration variables. $\beta_{n\times k}$ is the coefficient matrix and $\in_{m\times k}$ is the random error term.

3. Results and discussion

3.1. Characterization of Ag NPs

Ag NPs were prepared by sodium citrate reduction method, the resultant NPs were spherical (Fig. 1a) and with an average diameter of about 66 nm (Fig. 1b), and the size distribution generally conforms to the Gaussian distribution. UV–vis spectra (inset of Fig. 1b) showed the surface plasmon resonance (SPR) peak at 421 nm. FTIR spectroscopy confirmed the coordination of citrate on the Ag NPs surface, due to the stretch vibrations of C-O and COO$^-$ (with wavenumber shift) were

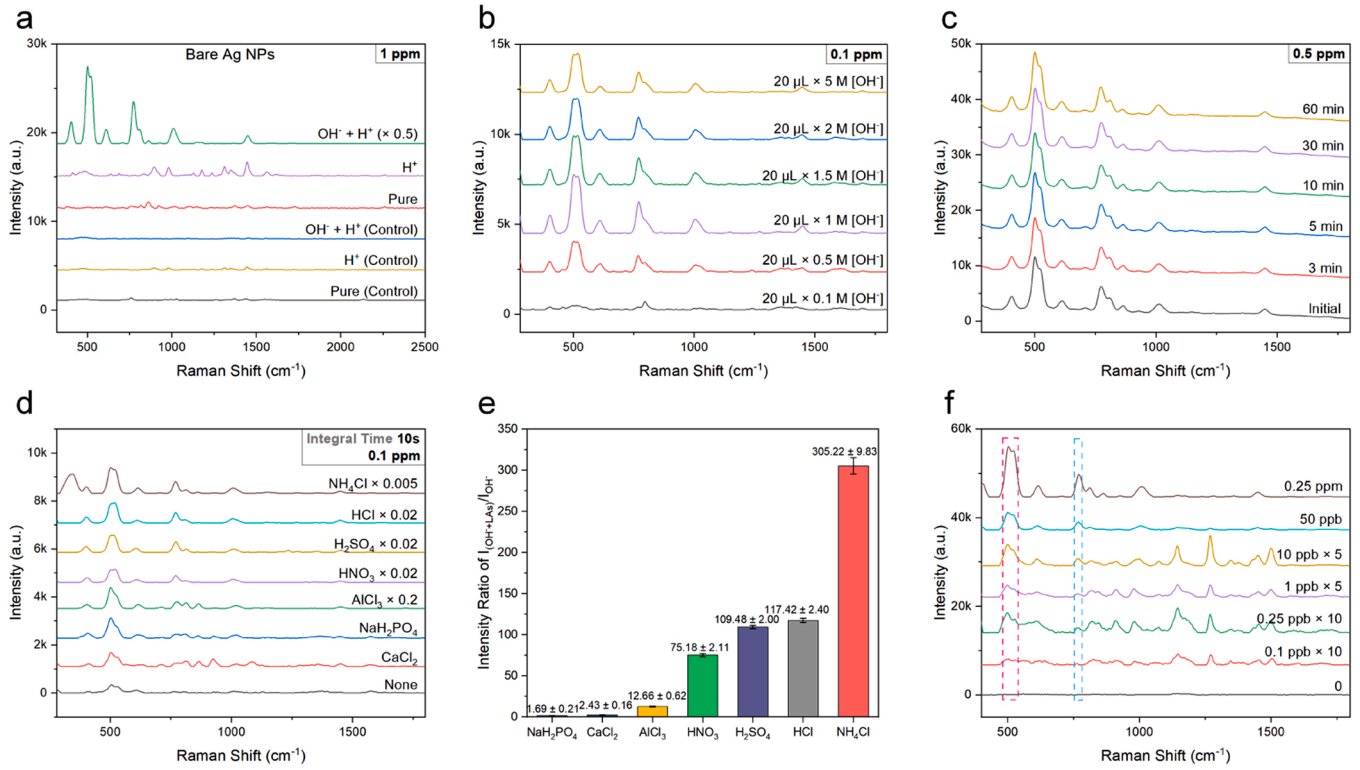


Fig. 2. (a) SERS spectra of MLT (1 ppm) obtained from different detection methods by Ag NPs. (b) Raman spectra of MLT (200 μL, 0.1 ppm) under different alkali amounts (20 μL, 0.1–5 M), the final pH of each group was adjusted to neutral by HCl (20 μL, 0.1–5 M). (c) SERS spectra of MLT (0.5 ppm) after different incubation times (0–60 min) in 0.1 M alkali. (d) The optimal SERS signals of MLT (0.1 ppm) hydrolysates after adjusting by different typically LAs, and the corresponding histogram of Raman intensity at peak 500 cm^{-1} (e), the error bars represent the standard deviation. (f) Evolution of Raman spectra with the increase of MLT concentrations from 0 to 0.25 ppm in pure water, the low concentration spectrum was magnified 5–10 times. The default laser power was 500 mW and the integration time was 5 s (except for Fig. 2d).

observed (Fig. 1c) and consistent with the previous studies [29,30].

XRD pattern (Fig. 1d) revealed the crystal structure of Ag NPs. Four distinct diffraction peaks were observed at 38.09°, 44.30°, 64.50° and 77.55°, corresponding to the Miller indices (111), (200), (220), and (311) respectively (JCPDS cards 04-0783) [31,32]. These lattice planes indicated that the Ag NPs were crystalline and in good agreement with the face-centered-cubic (FCC) structure. Notably, no diffraction peaks of silver oxide were observed (JCPDS cards 41-1104), indicated that the surface of the prepared Ag NPs was stable.

ICP-MS analyzed the Ag concentration of Ag colloid, and obtained a value of 108.868 mg/L (1.009 mM, this value is slightly higher than the concentration of precursor, probably due to the evaporation of a small amount of water during synthesis). Subsequently, the particle concentration of Ag NPs was calculated based on Eq. (3) by using a combination of average size and Ag concentration [33–35].

$$C_p = 3C_{mol}N_A V_s / 4\pi R^3 \quad (3)$$

where C_{mol} is the molarity of Ag (1.009 mM), N_A is the Avogadro constant, V_s is the volume of one Ag atom (0.017 nm^3, in FCC structure) and R is the average radius of Ag NPs. The calculated particle concentration of Ag NPs was 6.86×10^{10} particles/mL.

To ensure the applicability of Ag NPs in pesticide detection, malachite green (MG) was used to characterize the SERS enhanced performance. The corresponding normal Raman and SERS spectra are shown in Fig. S2 and the enhancement factor (EF) was calculated according to the formula (Eq. (4)):

$$EF = N_{bulk}I_{surf} / N_{surf}I_{bulk} \quad (4)$$

where I_{bulk} and I_{surf} represent the signal intensity in solution (normal Raman experiment) and nano-surface (SERS experiment), N_{bulk} and N_{surf} represent the number of measured molecules in solution and nano-surface excited by the laser beam, respectively. Finally, the EF of Ag NPs was calculated to be 1.98×10^8. The detailed calculation process of EF is available in the Supporting information.

The surface oxidation of Ag colloid during storage was studied by XRD, Fig. S3 shows the diffraction peaks of Ag colloids with different storage time (0, 4 and 9 months). No visible diffraction peaks of silver oxide were observed in all samples, owing to the presence of sodium citrate in the solution. Moreover, MG was used as the Raman probe molecule to explore the storage stability of Ag NPs. Fig. 1(e, f) shows the Raman response of freshly prepared Ag colloid to MG at different storage stages (0–30 days). The signal deviation in different periods were within 5% and no attenuation trend was observed, this indicated that the stable SERS performance of the Ag colloid.

3.2. Detection method and conditions optimization of MLT by using Ag NPs

In this study, the MLT was indirectly detected via hydrolysis with alkali and then by adjusting the detection conditions with LA as an assisted enhancer (AE). Fig. 2a shows the optimal SERS signals of MLT under different detection conditions. Significantly, the alkali hydrolyzed MLT with adjusted acidity (hydrochloric acid as the AE) exhibited the specific and highest signal compared with pure, acid hydrolyzed and alkali hydrolyzed. The pure and acid hydrolyzed MLT detection schemes were optimized from a series of different aggregators (Fig. S4) and acid concentrations (Fig. S5) respectively.

For the alkaline hydrolysis detection scheme, the alkali was used as a nucleophile to facilitate the hydrolysis, the LA was used to remove hydroxide and provide a protonic environment. Hence, the present of alkali and the influence of LA were the necessary investigation factors for

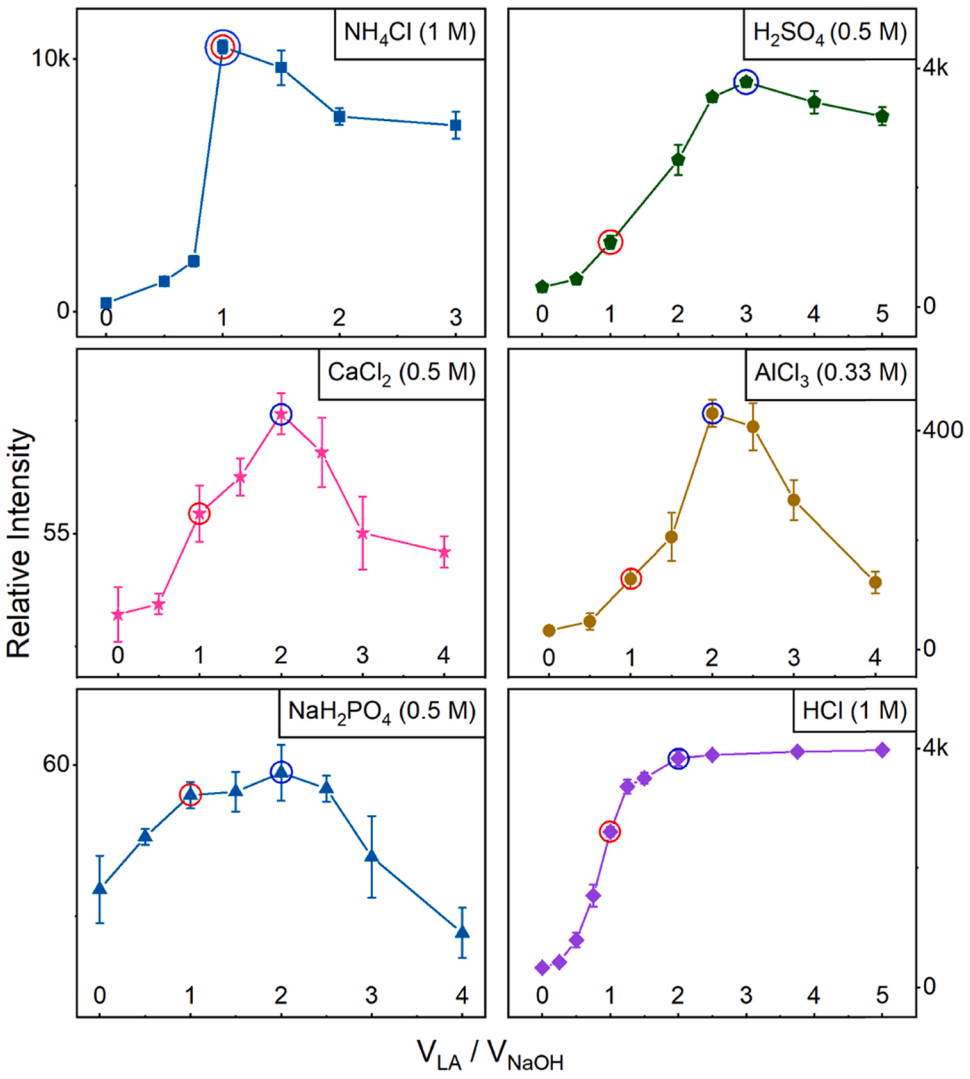


Fig. 3. The impact of different adding amounts of LA AEs on Raman intensity (500 cm^{-1}) under the same MLT (200 μL, 0.1 ppm) alkali hydrolysis condition. Among them, the concentrations of NH_4Cl and HCl were 1 M, the concentrations of $CaCl_2$, NaH_2PO_4 and H_2SO_4 were 0.5 M, the concentration of $AlCl_3$ was 0.33 M. Each X axis represent the ratio of adding volume of LA and adding volume of NaOH (20 μL, 1 M). The red circles indicate the alkali consumption points (i.e., the NaOH was completely reacted), and the blue circles indicate the highest signal points.

the detection of MLT. Fig. 2b shows the Raman signals of MLT standard sample (200 μL, 0.1 ppm) under different adding amounts of alkali (20 μL, 0.1–5 M) and the final pH were adjusted to neutral by HCl (NaOH (aq) + HCl (aq) → H_2O (l) + NaCl (aq), in a way of the same concentration and volume as alkali), the highest intensity was obtained at an adding amount of 20 mmol (1 M × 20 μL) of NaOH. Under this case, the detection condition was equivalent to sodium chloride as the aggregator to realize coupling effect, and no pure MLT signal (seen in Fig. S4) was observed. In other words, after alkaline hydrolysis, the complete decomposition of MLT was indicated. Moreover, after different incubation times (0–60 min) of MLT in the alkali (Fig. 2c), the almost constant SERS signals indicated that the alkaline hydrolysis completely occurred in the first instant.

Not only hydrochloric acid, we found that other Lewis acids (LAs) also can promote the signal elevation after MLT alkali hydrolysis, such as calcium chloride, aluminum chloride, sodium dihydrogen phosphate, nitric acid, sulfuric acid and ammonium chloride. Fig. 2d shows the optimal SERS signals of MLT hydrolysate after adjusting by different typical LAs. Compared with direct alkali hydrolysis, the SERS signals improved significantly after adding different LAs. According to their Raman intensity (500 cm^{-1}) (Fig. 2e), NH_4Cl possesses the most enhancement factor, up to about 305 times, and strong acids such as HCl and H_2SO_4 also have excellent improvement effect, as high as about 110 times.

Fig. 3 shows the impact of different amounts of adding LA AEs on Raman intensity (500 cm^{-1}) under the same MLT alkali hydrolysis condition. For NH_4Cl as LA AE, Raman strength increased with the LA amounts until the sodium hydroxide was completely reacted (alkali consumption point, red circle in Fig. 3), as shown in the following reaction:

$$NaOH\ (aq) + NH_4Cl\ (aq) \rightarrow NaCl\ (aq) + NH_3\ (aq) + H_2O\ (l)$$

For LA AEs that were easily ionized or alkali hydrolyzed to product protons such as HCl and $AlCl_3$, the Raman strength were found to increase with the increasing concentration of acidity, especially after completely reacting the sodium hydroxide, the Raman strength increased sharply and finally obtained the highest strength (highest signal points, red circles in Fig. 3) under an acidic condition. The related reactions are as follows:

$$NaOH\ (aq) + HCl\ (aq) \rightarrow NaCl\ (aq) + H_2O\ (l)$$

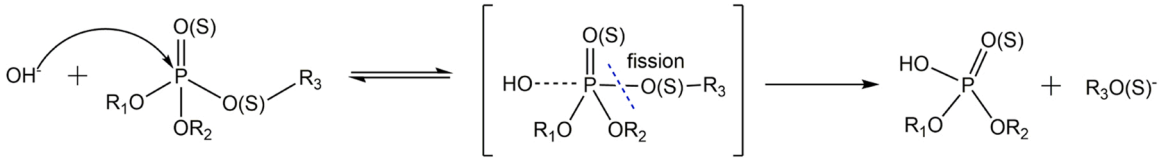
$$NaOH\ (aq) + H_2SO_4\ (aq) \rightarrow Na_2SO_4\ (aq) + H_2O\ (l)$$

$$NaOH\ (aq) + NaH_2PO_4\ (aq) \rightarrow Na_3PO_4\ (aq) + H_2O\ (l)$$

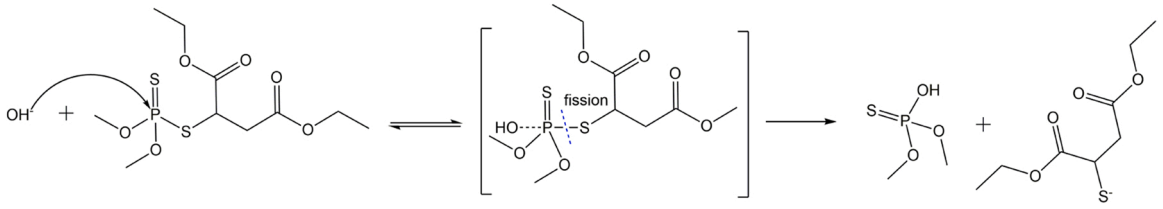
$$NaOH\ (aq) + CaCl_2\ (aq) \rightarrow NaCl\ (aq) + Ca(OH)_2\ (s)$$

$$NaOH\ (aq) + AlCl_3\ (aq) \rightarrow NaCl\ (aq) + Al(OH)_3\ (s)$$

These indicated that the removal of hydroxide ions and the provision of proton environment were beneficial to the detection of alkali



Scheme 1. The common alkaline hydrolysis pathway of organophosphorus molecules, following the S_N2 substitution reaction.



Scheme 2. In the case of quasi Scheme 1, the assumed alkali hydrolysis pathway of MLT.

hydrolysates of MLT, which resulted in a stronger competitive advantage of the thiol group in the hydrolysates on the silver surface.

Based on the above-optimized conditions, the Raman spectra of MLT at different concentrations in pure water were obtained (Fig. 2f). Intensity above 3 times of signal to noise ratio (SNR) was considered as the threshold of detection limit, so the LOD of MLT in water was determined to be 0.1 ppb. This value is approximately 500 times smaller than that of the detection limit of pure MLT (50 ppb, Fig. S6), indicating the obvious sensitivity advantage of the alkaline hydrolysis scheme.

3.3. Mechanism of MLT alkaline hydrolysis

As we know, many organophosphorus pesticide molecules, such as malathion, methidathion, parathion and fenitrothion etc., can be hydrolyzed under alkaline conditions. Generally, hydroxide ion can act as a nucleophile to attack the central P atom in phosphate ester group ensue the P—O(S) bond cleavage through addition-elimination mechanism (Scheme 1) [36–39]. According to this pathway, the alkaline hydrolysis of MLT generates DMTP and 1, 4-diethyl ester n-butyl thiol (DEBT) (Scheme 2), which was also the scheme that has been widely recognized in many recent reports [16–18]. However, the SERS signal and GC-MS result shows that what were generated were DMDTP and 1, 4-diethyl ester n-butene (DEBN). Fig. 4a shows the SERS spectra of MLT after alkali hydrolysis with HCl as AE. It was found that, the characteristic peak was highly coincident with DMDTP standard sample and no DMTP signal was observed. GC-MS (Fig. 4b) confirmed the existence of DMDTP (157 *m/z*) and DEBN (173 *m/z*) at approximately 4 and 9 min (Fig. S7), respectively. This indicated that the alkaline hydrolysis of MLT followed the Scheme 3, which is a β-elimination reaction (Hofmann rule). This is mainly due to the presence of the electron-withdrawing group (carbonyl) on the adjacent β-C, resulted in a decrease in the electronegativity of β-C, which strengthened the acidity of β-H and made it more readily to be captured by the nucleophile to break the C—H bond. Corresponding molecular structure and electrostatic potential map are shown in Fig. 4c. And with the electrons push, on the α-C, the leaving group ($[DMDTP]^-$) leaves with a pair of electrons. In parallel, the α-C also adjacent an electron-withdrawing group, which facilitates the formation of $\alpha\text{-}C^+$, further facilitating the above process. In addition, we detected several other typical dithiophosphate ester organophosphorus pesticide molecules, such as fonofos, phorate, dimethoate, methidathion, phosalone and azinophos-ethly, and no DMDTP signal was observed (Fig. 4d). As shown in Fig. 4e, these molecular structures lack the following two prerequisites to activate the β-elimination reaction. (1) The leaving group must be connected to an alkyl group. (2) The presence of β-C and its adjacent electron-withdrawing group, and the number of protons on β-C is greater than that of on α-C, ensuring that β-H is more acidic than α-H. Hence, they preferentially perform S_N2 substitution at the central P atom in alkaline condition (seen to Scheme 1). For example, methidathion alkali hydrolysis occurs with the P-S bong cleavage and produced the DMTP and thiadiazole derivative (Scheme S1). Moreover, due to other organophosphorus pesticides such as triphosphate and monothiophosphate organophosphorus have no pathway to produce DMDTP in alkaline condition. Hence, MLT was indirectly detected by β-elimination product of MLT under alkaline condition.

3.4. Mechanism of the detection

The detection mechanism was analyzed by using HCl and NH_4Cl as LA AE, represented free proton environment and ammonium ion environment respectively.

Since the SERS signal of the alkaline hydrolysates of MLT was almost completely coincident with that of DMDTP standard sample, this indicated that DEBN (another hydrolysate) does not contribute to the Raman signal in this detection method due to the lack of effective adsorption group for Ag NPs. Therefore, DMDTP was considered as the main research object in the detection mechanism.

To confirm the attribution of SERS characteristic peaks of MLT alkali hydrolysates, DFT calculation was performed to investigate the Raman features of DMDTP (Fig. 5a). Table 1 shows the attributions of skeletal vibration for DFT simulation and SERS experiment spectrum. The skeletal vibration associated with the sulfur-phosphorus bond occurred at 611, 522, and 500 cm^{-1}, which were referred to two binding states of the sulfur-phosphorus group on the surface of Ag NPs, as shown in Fig. 5b. For model 1, when only the thiol group was bonded to the Ag NPs surface, P-S and P═S stretching vibration were observed at 500 and 611 cm^{-1}, respectively. For model 2, based on model 1, the P═S bond was broken and returned one electron to each of the P and S (formed S^-) atom. Thus, both P-S groups were coordinated to Ag NPs surface together. Apparently, these P—S bonds have a higher electron density than that of model 1, showed a blue shift result (522 cm^{-1}).

For the case of HCl as the LA AE, a transition relationship between the above two model states was observed, which were affected by the proton environment and MLT concentration. Fig. 5c highlights the peak intensity of 611 and 522 cm^{-1} under a series of acidity conditions, and the ratio of average peak intensity I_{611}/I_{522} was calculated. The ratio decreased with the increase of acidity, indicated that part of P═S vibration transferred to P-S vibration (P1 process in Fig. 5b). This can be explained by the proton-induced P═S bond stretching, due to the HOMO orbit of DMDTP molecule mainly localizes on the P═S bond (Fig. S8), which makes the P═S bond more susceptible to the electrophile, occurring the metal-ligand charge transfer (CT). In parallel, the

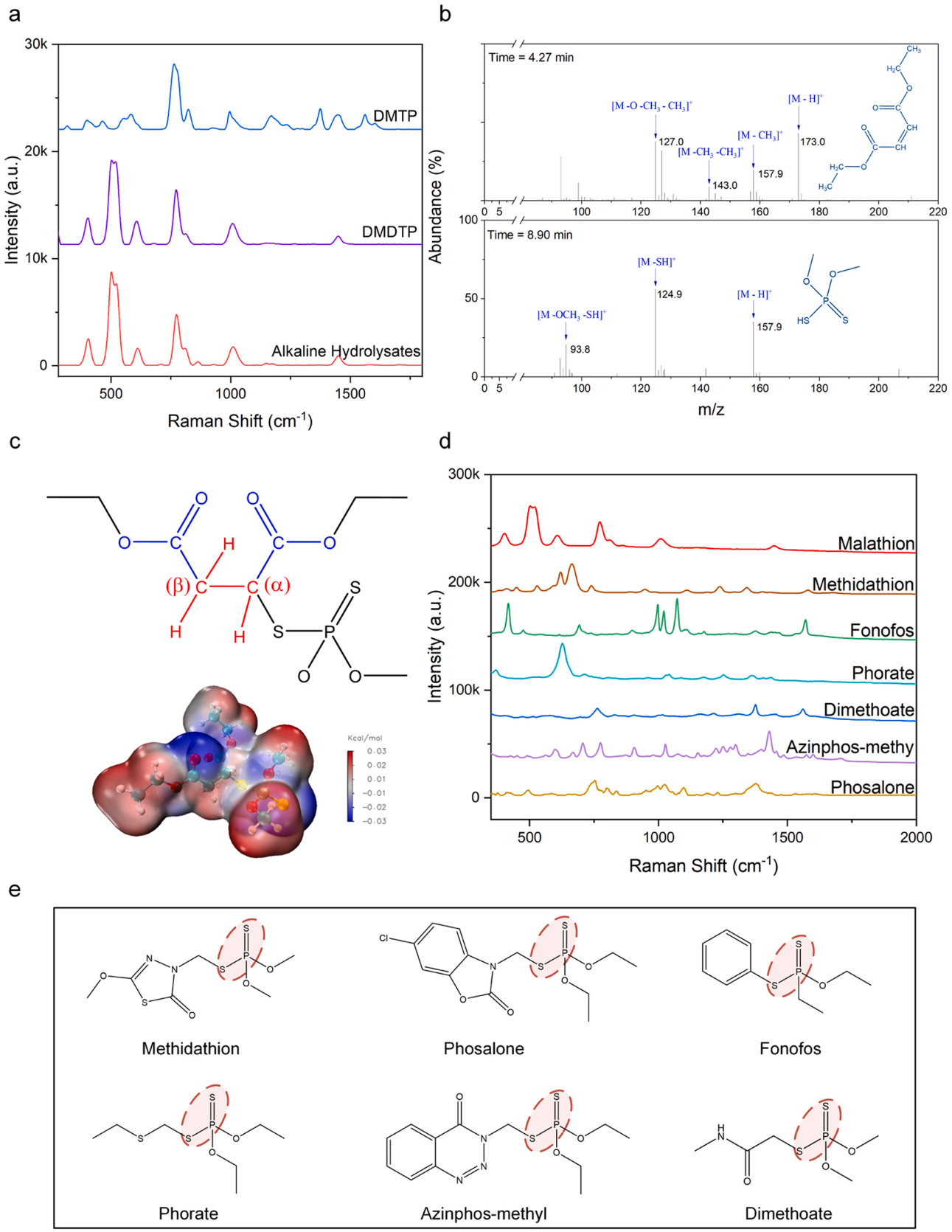
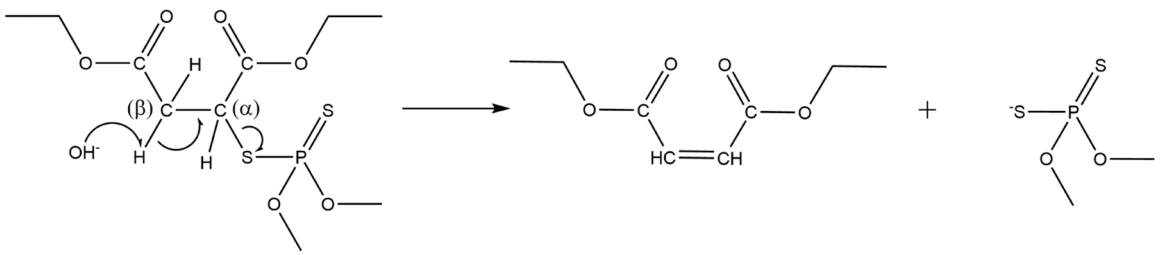


Fig. 4. (a) SERS spectrum of MLT alkaline hydrolysates, DMDTP and DMTP. (b) GC-MS result of MLT hydrolysates. (c) Molecule plan structure (the blue areas represent high electron density; the red area represents low electron density) and mapped molecular electrostatic potential for MLT. (d) SERS spectrum of different dithiophosphate ester organophosphorus pesticide molecules under the same alkali hydrolysis and detection condition. (e) Plan structures of six kinds of typical dithiophosphate ester organophosphorus pesticide molecules.



Scheme 3. The alkaline hydrolysis of MLT generates DEBN and DMDTP, following the β-elimination reaction.

protonic environment was favorable for the thiol group to bind to silver through nucleophilic reaction. All of these resulted in the increase of model 2. Moreover, both of the CT process and bonding effect can contribute to promoting chemical enhancement [40–42]. This is why the acidity at the highest signal point was higher than the alkali consumption point (Fig. 3) for HCl, $AlCl_3$, etc. as the LA AEs. Different MLT concentrations were found to have a significant influence on the intensity relationship between the 500 and 522 cm^{-1}. Fig. 5d highlights the Raman spectra of MLT hydrolysates at different concentrations, it can be seen that as the concentration increased, the peak intensity at 500 cm^{-1} became higher than that at 522 cm^{-1}. This change phenomenon also occurred in the DMDTP standard samples (Fig. S9). So, this may be due to the competitive adsorption behavior between the two binding states of DMDTP. As the MLT concentration increased, more dissociative DMDTP molecules competed for the P-S-Ag binding site on the nano-silver surface, which promoted model 2 to release one of the binding sites to reduce the nano-surface occupied area (seen in the inset of Fig. 5d). Thus, model 2 was converted to model 1 and resulted in a higher peak strength ratio of I_{500}/I_{522} (P2 process in Fig. 5b). To further verify this competition pathway, another three analogous molecules (TGA, L-cysteine and cysteamine), with thiol groups and no obvious SERS respond, were added to the hydrolysis products of MLT. Fig. S10 shows the effects of different concentrations of the additives on the signal at a fixed concentration of MLT hydrolysates. The peak strength ratio of I_{500}/I_{522} was increased with the increase of additives concentration, demonstrated that model 2 released one of the P-S-Ag binding sites. These revealed that the binding state of DMDTP on the silver surface was susceptible to the influence of the competing molecules, resulted in the conversion of model 2 to model 1.

As we know, in the case of NH_4Cl as the LA AE, the ammonium ions were converted to ammonia molecules in the presence of sodium hydroxide (i.e., NaOH (aq) + NH_4Cl (aq) → NaCl (aq) + NH_3 (aq) + H_2O (l)). Meanwhile, the SERS signal of alkaline hydrolysates of MLT was greatly enhanced compared with other AEs. To illustrate the role of ammonium and ammonia molecules in signal enhancement. A comparative experiment was performed by adding ammonium chloride and ammonia to DMDTP standard samples (sodium chloride as aggregator and blank control), respectively. Fig. S11 shows that the signal intensity of the ammonia group was significantly enhanced, while that of the ammonium chloride group was close to that of the control group, suggesting that the additional enhancement was mainly caused by ammonia molecules. This is due to the formation of silver ions with vacant orbital (5 s) after the bonding reaction (caused by capping agent and analyte) on the surface of Ag NPs, and these silver ions were easily attracted and enriched ammonia molecules on the surface of Ag NPs via coordination effect (due to the presence of lone pair electrons of ammonia), while not the ammonium ions. Moreover, as the lone pair of electrons on nitrogen atom participate in the coordination with silver ion, the electron density of each H atom in the N—H bonds decreases, so that the H atoms were more eager for electrons and easier to form hydrogen bonds. These created the favorable conditions for the formation of hydrogen bonds (P═S···H-N) complexation of DMDTP with ammonia on the surface of Ag NPs, which changed the binding configuration of analyte and increased the effective Raman scatting cross-section, defined as model 3 (P3 process in Fig. 5b). Model 3 presented the same signal as model 1, and significantly reduced the formation of model 2, showed a decrease strength of the 522 cm^{-1} (Fig. 5e). Furthermore, in contrast to other LA AE, the addition of protons did not make the signal stronger (Fig. 5 f1), and the value of I_{500} / I_{522} increased (Fig. 5 f2). At this point, the ammonia molecule was converted to ammonium ion (i.e., NH_3 (aq) + HCl (aq) → NH_4Cl (aq)). This is because of the consumption of ammonia molecules and the increase of proton concentration were not conducive to the formation of DMDTP complexation, but was conducive to the formation of Model 2 (P4 process in Fig. 5b), resulted in a smaller Raman scattering cross-section of the probe molecule on the nano-surface. This is also one of the reasons that the alkali consumption point was the highest signal point in Fig. 3 for NH_4Cl as the LA AE.

The above analysis shows that the analyte concentration, ionic atmosphere and other surface-competitive molecules have affected the binding states of the hydrolysis products on the silver surface, resulted in a significant change in the Raman signal. These mechanisms helped to explain the influence of matrix molecules on detection results in the actual application (Section 3.6), which were important to the evaluation of characteristic variables and the selection of algorithms in quantitative analysis (Section 3.7). Interestingly, the systematic theoretical and applied approach is not only applicable to the research object of this paper, but also can provide a valuable reference for future study on other similar molecules.

3.5. Determination method and conditions optimization for MLT in tea

The flow chart of the pre-treatment and detection steps of MLT in the tea sample can be seen in Fig. S12a. Compared to the complex operation steps and long operation time required for the existing HPLC/MS-HPLC detection technology (Fig. S12b), this study only need three operation steps and complete the whole experimental process (including the detection result output) within 5 min, and the experimental cost is less than 3% of the former. The basic strategy was using the dispersive solid-phase extraction (DSPE) method [43] to clean the interfering substances, which were selectively retained on the sorbent, and the supernatant was used for analysis. In brief, the MLT was extracted from tea by acetonitrile and purified by graphitized carbon, and then detected by the above-mentioned alkaline hydrolysis method. Fig. S13a reflects the extraction effect of different solvents. Among them, acetonitrile and acetone as extraction agents both show good signal intensity output results. However, the solvent peak of acetone (800 cm^{-1}) has obvious interference with the important characteristic peaks of probe molecules (770 cm^{-1}), which lead to a great influence on the accuracy of the quantitative analysis. Hence, acetonitrile was selected as the extraction agent. Fig. S13b shows the matrix removal effect of different weights of GCB as a purifier, 10 mg per 0.2 g of tea sample was selected as the optimal weight. Due to the amounts of organic acids and non-polar substances contained in tea, PSA and C18 were added into GCB, respectively, to improve the purification efficiency. However, Fig. S13c reflects that the addition of PSA and C18 have no significant effect on signal sensitivity improvement. Moreover, the QuEChERS method [44] was introduced to demonstrate that PSA and C18 were not enough

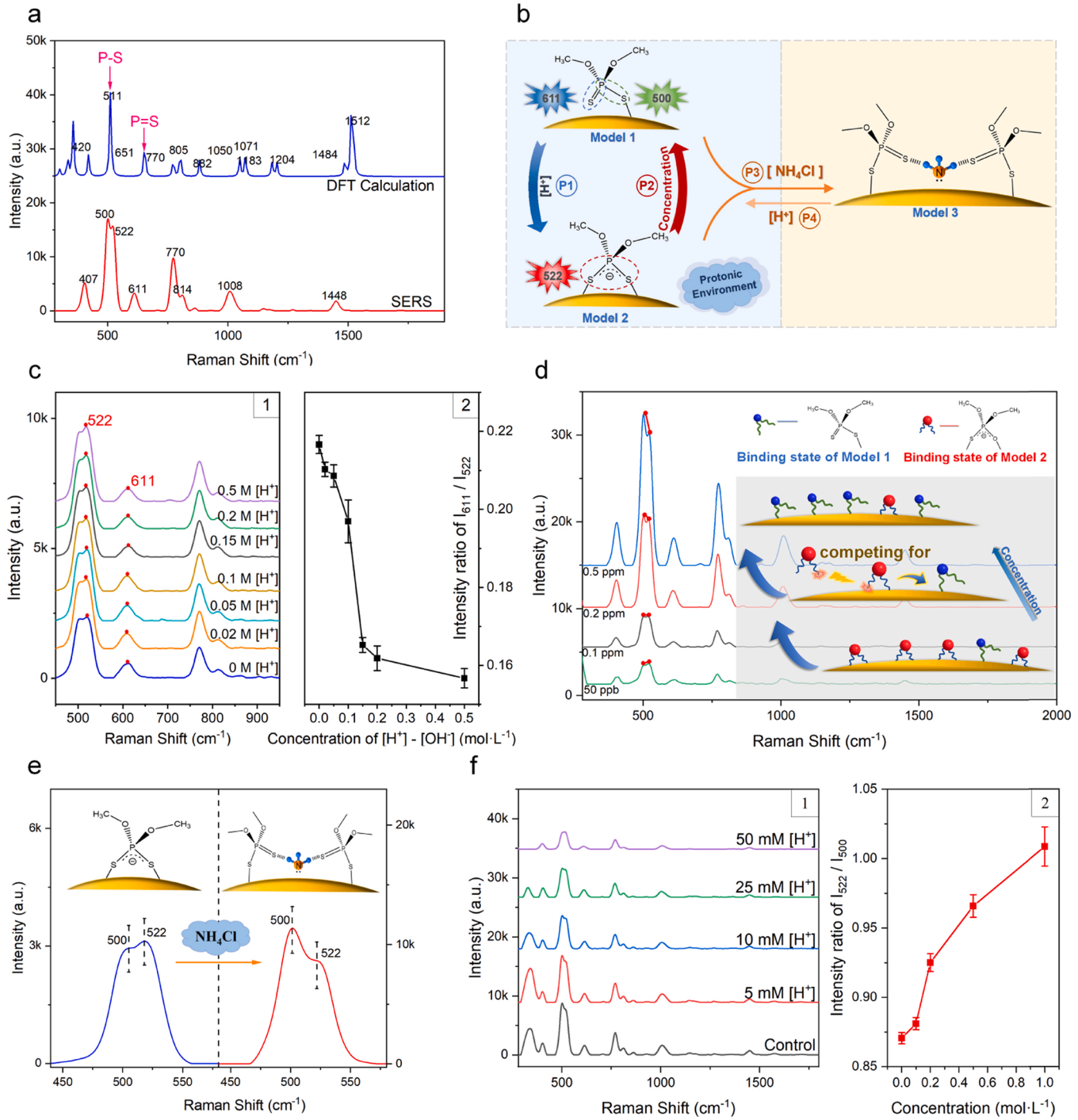


Fig. 5. (a) B3LYP/6–31 +G(d) computed Raman spectrum and SERS spectrum of DMDTP. (b) Three binding models and conversion pathways (P1-P4) of DMDTP on Ag NPs surface in the protonic and amine ions environment. (c) Raman peaks feature at 522 and 611 cm^{-1} under a series of acidic conditions (the curve of the average intensity ratio of I_{611}/I_{522} change with the corresponding acidity). (d) The intensity relationship between 500 and 522 cm^{-1} at different concentrations of MLT, the slop line between the red dots represents the peak ratio, the inset illustrates the process of free DMDTP molecules compete with model 2 and generate model 1. (e) Changes of signals and binding models with HCl and NH_4Cl as AEs, respectively. (f) With NH_4Cl as AE, the effect of adding different concentrations of HCl on the SERS signal, and the ratio of peak intensity at 522 and 500 cm^{-1}. In addition, (c-f) were related to the P1-P4 processes respectively.

effective in removing matrix interference. This directly demonstrated the importance and necessity of GCB for the removal of matrix effects in tea in this method. Finally, to meet the conditions for the detection by using silver nanoparticles, the sample in the acetonitrile phase was diluted into the aqueous phase (Fig. S13d), and a 5 times dilution showed the best signal response. Under the optimized conditions, qualitative and quantitative analysis of MLT in tea was performed.

3.6. Application diversity and detection limit in tea

Fresh tea leaves and nine kinds of processed tea samples (white tea, green tea, oolong tea, and black tea) (Fig. 6a) with different fermentation processes were used as experimental subjects. Fig. 6b shows the Raman spectrum of various tea samples with MLT added (0.5 ppm, and the corresponding control groups can be seen in Fig. S14), every

Table 1
The SERS experimental observed frequencies of skeletal vibration for MLT hydrolysates and B3LYP/6–31 +G(d) calculated frequencies of DMDTP.

SERS (cm^{-1})	DFT calculation (cm^{-1})	Mode descriptions
407	420	P-O-C shear vibration
500	511	P-S stretching vibration
522	–	P-S stretching vibration
611	651	P═S stretching vibration
770	770	Per P-O stretch of P–O–C symmetric stretching vibration
814	805	Per P-O stretch of P–O–C asymmetric stretching vibration
1008	1050	P–O–C symmetric deformation
1448	1486	C-H bending vibration of -CH3
–	1512	C-H stretching vibration of -CH3

spectrum contains all of the main characteristic peaks measured in the standard sample, this indicated that the detection method established in this study is applicable to different kinds of tea. To briefly explain the detection limit of this method, we only used the black tea as the experimental sample, and a serial of different concentrations (0–10 ppm) of MLT spiked samples were measured (Fig. 6c). It was found that different concentrations of MLT showed a highest characteristic peak at 500 cm^{-1}, this was due to the ammonium chloride and sulfhydryl matrix molecules of tea inhibiting DMDTP from producing the model 2 binding state on the nano-surface, which decreased the peak intensity at 522 cm^{-1} and increased at 500 cm^{-1}. For this strongest peak, the signal above 3 times SNR was observed for the sample at 0.05 ppm. This concentration can be defined as LOD, which is ten times lower than MRL required by China, Japan and the European Union.

Table 2 summarizes the performance of previous SERS-based reports on the detection of MLT as compared to this work. Surprisingly, in a previous work [16], SERS active Ag nanostructure substrate was prepared by electrochemical method in 8 M KOH solution for MLT hydrolysate detection under the same alkaline condition. They have obtained a LOD of 10 pM (~3.5 ppt), which was about 30 times lower than that of this work. Apart from the extra electromagnetic and chemical enhancement provided by electrochemical SERS (EC-SERS) technology

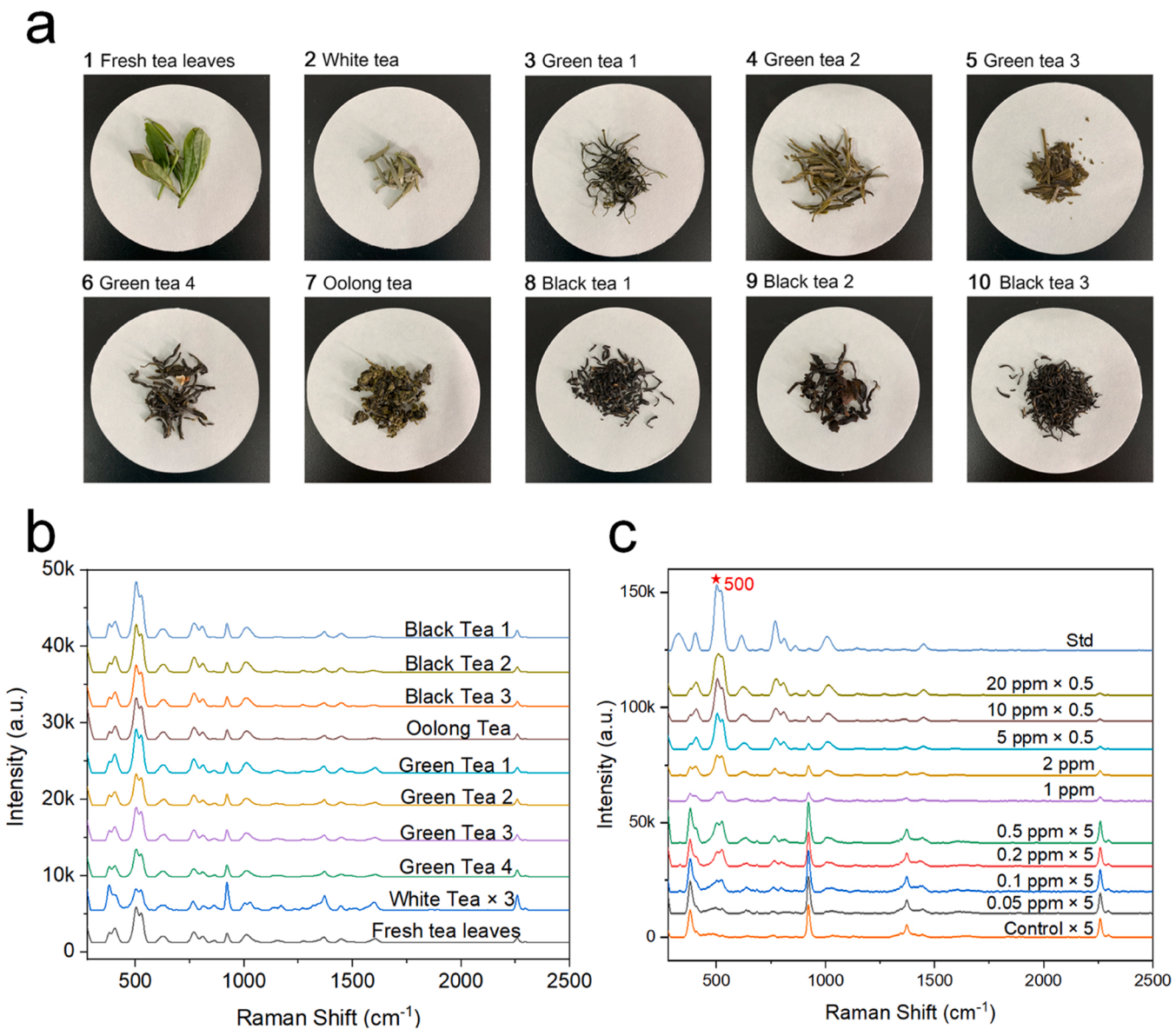


Fig. 6. (a) Images of different tea samples used in the application experiment. (b) Raman spectra of different tea samples with MLT added (0.5 ppm). (c) Evolution of Raman spectra with the increase of MLT concentration from 0 to 20 ppm in black tea, the low concentration spectrum was magnified 5 times.

Table 2
The performance and comparison of previous reports on the detection of MLT by SERS methods.

Ref.	Substrates	Detection and assistant methods	Detection objects	Sensitivity	
				STD	Actual application
This work	Spherical Ag NPs colloid	SERS	Alkaline hydrolysates using NH_4Cl as AE	0.1 ppb	50 ppb (In black tea)
[12]	Nanoporous microfluidic matrix	SERS	Pure MLT	12 ppb	No Mention
[13]	Ag-NP-loaded filter membrane	SERS	Pure MLT	61.5 ppb	No Mention
[14]	Ag NPs inkjet-printed paper	SERS	Pure MLT	82.6 ppb	No Mention
[15]	Ag NPs@spermine colloid	SERS	Pure MLT binding aptamer	0.5 μM	No Mention
[16]	Nano-silver modified electrode	SERS combined with electrochemistry	Alkaline hydrolysates	10 pM	No Mention

[45], we consider this was caused by the following three reasons: 1) The positive electrode enhances the attraction of surface silver to electron-rich groups, resulting in the enrichment of MLT hydrolytic products on the surface of silver; 2) The volume of detection solution was about 50 times that of our study, namely, the number of probe molecules at the detection limit concentration was about 1.7 times more than that of our study; 3) The detection time for low concentration molecules reached 300 s, which was 60 times of the maximum integration time in this paper. In other words, our approach has higher SERS response for single target molecule and the strategy is more consistent with the surface selection rule [46,47]. Actually, the EC-SERS method was always considered to be one of the most complicated system in SERS, it provides greater flexibility for studying interface structures and mechanisms, rather than applications [45]. Here, our research has great advantages in terms of operation, time consumption and cost, while meeting the requirements of highly sensitive and instant detection, which is suitable for further applied research and is the only reported method that has been applied to real samples.

3.7. Quantitative analysis of MLT in tea sample

In order to satisfy the statistical reliability, 211 samples' SERS spectra distributed in different concentrations were collected and their baseline correction was performed. Fig. S15a shows the average spectra of MLT addition samples with different concentrations. Five characteristic peaks (407, 500, 522, 611, and 770 cm^{-1}) were selected as univariate/multivariate fitting objects, the intensity of each peak was normalized by the matrix peak at 922 cm^{-1}, and read automatically by a self-developed program written on MATLAB. To clearly identify each peak, the minimum spiked concentration of MLT was set at 0.1 ppm. Then the univariate/multivariate linear regression (ULR/MLR) equation of Raman characteristic peak intensity and concentration of MLT in tea was established. Fig. S15(b–f) presents the univariate linear fitting results of five individual characteristic peaks intensity at 0.1–5 ppm MLT concentration (results above 10 ppm were not conducive to a good linear relationship, as shown in Fig. S16). The 407 and 770 cm^{-1} peaks have better determination coefficient of ULR equation than that of 500, 522 and 611 cm^{-1} peaks. According to the above theoretical analysis, this is due to the target molecules, organic acids and other surface-competitive molecules can affect the peaks strength at 500, 522 and 611 cm^{-1}. In parallel, there was no obvious evidence that the peaks of 407 and 770 cm^{-1} (attributed to P-O-C shear vibration and P-O stretching vibration of DMDTP) were affected by the above factors. However, this did not exclude the possibility that a single characteristic peak as a fitting variable was easily affected by external interference factors. Hence, MLR modeling method, which uses the least square method to estimate the coefficient vector and assigns different weights for each characteristic peak, was applied to solve the problems of quantitative analysis caused by complex peak intensity variations in practical application detection. As shown in Table 3, the linear regression equations based on the intensity of single to multiple characteristic peaks were summarized. Found that: (1) In the combinations of equal number of characteristic peaks, the linear regression equation with 407 or 770 cm^{-1} peak as variable has a higher determination coefficient, this indicates that a good linear fitting variable in ULR will help to generate a high determination coefficient in MLR; (2) In the combinations of different number of characteristic peaks, the more the designated peaks fitted, the larger the correlation coefficient obtained, this due to the MLR can use more peaks information and better explain the concentration information. Finally, the MLR equation with five characteristic peaks as variables, which possesses the highest determination coefficient (R^2 =0.9573), was selected as the optimal quantitative equation (Y=0.0006 *x1 + 0.0001 *x2 + 0.0004 *x3–0.0009 *x4–0.0011 *x5). Compared with the ULR modeling method, the MLR modeling method was more suitable for accurate quantitative analysis.

Then, five groups of parallel experiments were carried out to calculate the recovery rate under the MLR modeling method. As shown in Table S1, the recoveries of different MLT spiked samples were between 90% and 105%, which indicated that the MLR modeling method was suitable for the quantitative analysis of MLT in tea based on the detection method proposed by this study.

4. Conclusions

In this work, spherical Ag NPs were used as SERS substrate to detect the alkali hydrolysates of MLT, obtained a distinctive SERS signal compared with pure MLT detection scheme and other reports, and the analyte was detected up to ppb level (0.1 ppb in water). The alkaline hydrolysis process of MLT was analyzed and confirmed that the hydrolysates with SERS response was DMDTP. According to the influence of different LAs on the Raman signal of alkaline hydrolysate, the addition of LA was the most important factor to realize the highly sensitive detection. Significantly, the complexation of the target hydrolysate with ammonia (formed by ammonium chloride), resulted in about 305 times additional enhancement compared with non-LA AE group. By investigating the variations of LAs, acidity, analyte concentration and external interference molecules on the Raman signal of MLT alkaline hydrolysate, three binding models of hydrolysate molecules on the surface of nanoparticles were proposed and their transformation relationships were revealed for the first time. A three-step operation method, which only need 5 min, was developed for the detection of MLT in different tea samples, up to the detection limit of 50 ppb in black tea. In this practical application, the MLR model of quantitative analysis was established from five characteristic variables, and a good dynamic range was obtained in the range of 0.1–5 ppm. To our knowledge, this is the only report on the detection of MLT in tea samples, with the characters of high sensitivity, strong reliability, short time consuming, low cost and simple operation. Hence, the detection method, mechanism and algorithm will provide new ideas for other molecular detection, which is of great significance in food safety, environmental monitoring and clinical application.

CRediT authorship contribution statement

Xiaojing Chen: Resources, Writing – review & editing, Supervision, Funding acquisition. **Xixi Huang:** Software, Formal analysis, Validation, Visualization, Investigation, Data curation. **Shiliang Chen:** Conceptualization, Methodology, Investigation, Writing – original draft, Writing –

Table 3
The determination coefficients and linear regression equations for ULR and MLR. The boldfaces represent the optimal combinations of the equal number of characteristic peaks.

Variables	R^2	linear equations
407	0.9233	$Y = 1.7742 * 10^3 * x$
500	0.8997	$Y = 4.9881 * 10^3 * x$
522	0.9233	$Y = 4.1812 * 10^3 * x$
611	0.9089	$Y = 896.3276 * x$
770	**0.9293**	$Y = 1.4489 * 10^3 * x$
407 + 500	0.9286	$Y = 0.3993 * 10^{-3} * x1 + 0.0574 * 10^{-3} * x2$
407 + 522	0.9329	$Y = 0.2876 * 10^{-3} * x1 + 0.1186 * 10^{-3} * x2$
407 + 611	0.9330	$Y = 0.4099 * 10^{-3} * x1 + 0.2980 * 10^{-3} * x2$
407 + 770	**0.9378**	$Y = 0.3520 * 10^{-3} * x1 + 0.2540 * 10^{-3} * x2$
500 + 522	0.9273	$Y = -0.1223 * 10^{-3} * x1 + 0.3834 * 10^{-3} * x2$
500 + 611	0.9238	$Y = 0.0641 * 10^{-3} * x1 + 0.7699 * 10^{-3} * x2$
500 + 770	0.9285	$Y = 0.0448 * 10^{-3} * x1 + 0.5193 * 10^{-3} * x2$
522 + 611	0.9314	$Y = 0.2109 * 10^{-3} * x1 + 0.1219 * 10^{-3} * x2$
522 + 770	0.9366	$Y = 0.5520 * 10^{-3} * x1 - 0.8726 * 10^{-3} * x2$
611 + 770	0.9327	$Y = 0.5586 * 10^{-3} * x1 + 0.3359 * 10^{-3} * x2$
407 + 500 + 522	0.9407	$Y = 0.2802 * 10^{-3} * x1 + 0.0006 * 10^{-3} * x2 + 0.1188 * 10^{-3} * x3$
407 + 500 + 611	0.9390	$Y = 6.4849 * 10^{-4} * x1 + 1.7853 * 10^{-4} * x2 - 0.0011 * x3$
407 + 500 + 770	0.9417	$Y = 4.7642 * 10^{-4} * x1 + 1.3835 * 10^{-4} * x2 - 3.5035 * 10^{-4} * x3$
407 + 522 + 6111	0.9430	$Y = 0.3699 * 10^{-3} * x1 + 0.1874 * 10^{-3} * x2 - 0.4966 * 10^{-3} * x3$
407 + 522 + 770	**0.9536**	$Y = 3.1983 * 10^{-4} * x1 + 5.3188 * 10^{-4} * x2 - 0.0012 * x3$
407 + 611 + 770	0.9432	$Y = 0.3368 * 10^{-3} * x1 + 0.0385 * 10^{-3} * x2 + 0.2497 * 10^{-3} * x3$
500 + 522 + 611	0.9385	$Y = -0.1096 * 10^{-3} * x1 + 0.3342 * 10^{-3} * x2 + 0.1677 * 10^{-3} * x3$
500 + 522 + 770	0.9423	$Y = -1.4819 * 10^{-4} * x1 + 7.8692 * 10^{-4} * x2 - 0.0010 * x3$
500 + 611 + 770	0.9328	$Y = 0.0153 * 10^{-3} * x1 + 0.5358 * 10^{-3} * x2 + 0.2997 * 10^{-3} * x3$
522 + 611 + 770	0.9506	$Y = 5.7283 * 10^{-4} * x1 + 2.0830 * 10^{-4} * x2 - 0.0010 * x3$
407 + 500 + 522 + 611	0.9481	$Y = 0.5807 * 10^{-3} * x1 + 0.1592 * 10^{-3} * x2 + 0.0064 * 10^{-3} * x3 - 0.9279 * 10^{-3} * x4$
407 + 500 + 522 + 770	0.9536	$Y = 3.1073 * 10^{-4} * x1 - 1.0027 * 10^{-5} * x2 + 5.4886 * 10^{-4} * x3 - 0.0012 * x4$
407 + 500 + 611 + 770	0.9525	$Y = 8.1002 * 10^{-4} * x1 + 2.9257 * 10^{-4} * x2 - 0.0012 * x3 - 5.4826 * 10^{-4} * x4$
407 + 522 + 611 + 770	**0.9558**	$Y = 4.0820 * 10^{-4} * x1 + 6.0027 * 10^{-4} * x2 - 4.8241 * 10^{-4} * x3 - 0.0012 * x4$
500 + 522 + 611 + 770	0.9472	$Y = -1.4436 * 10^{-4} * x1 + 7.5756 * 10^{-4} * x2 + 2.6186 * 10^{-4} * x3 - 0.0011 * x4$
407 + 500 + 522 + 611 + 770	**0.9573**	$Y = 0.0006 * x1 + 0.0001 * x2 + 0.0004 * x3 - 0.0009 * x4 - 0.0011 * x5$

review & editing, Data curation. **Shujat Ali:** Writing – original draft, Writing – review & editing. **Xi Chen:** Validation. **Leiming Yuan:** Visualization. **Wen Shi:** Resources, Writing – original draft. **Guangzao Huang:** Visualization, Software.

Declaration of Competing Interest

The authors declare that they have no known competing financial interests or personal relationships that could have appeared to influence the work reported in this paper.

Acknowledgments

This work was supported by the Natural Science Foundation of Zhejiang Province [LY21C200001], National Key Research and Development Program of China [2017YFD0401302].

Appendix A. Supplementary material

Supplementary data associated with this article can be found in the online version at doi:10.1016/j.snb.2022.131584.

References

[1] M. Yeganeh, A. Azari, H.R. Sobhi, M. Farzadkia, A. Esrafili, M. Gholami, A comprehensive systematic review and meta-analysis on the extraction of pesticide by various solid phase-based separation methods: a case study of malathion, Int. J. Environ. Anal. Chem. 101 (2021) 1–18, https://doi.org/10.1080/03067319.2020.1867721.
[2] M. Kermani, M. Dowlati, M. Gholami, H.R. Sobhi, A. Azari, A. Esrafili, M. Yeganeh, H.R. Ghaffari, A global systematic review, meta-analysis and health risk assessment on the quantity of Malathion, Diazinon and Chlorpyrifos in vegetables, Chemosphere 270 (2021), 129382, https://doi.org/10.1016/j.chemosphere.2020.129382.
[3] C. Li, H. Zhu, C. Li, H. Qian, W. Yao, Y. Guo, The present situation of pesticide residues in China and their removal and transformation during food processing, Food Chem. 354 (2021), 129552, https://doi.org/10.1016/j.foodchem.2021.129552.
[4] A.R.C. Braga, V.V. de Rosso, C.A.Y. Harayashiki, P.C. Jimenez, Í.B. Castro, Global health risks from pesticide use in Brazil, Nat. Food 1 (2020) 312–314, https://doi.org/10.1038/s43016-020-0100-3.
[5] Z. Hua, T. Yu, D. Liu, Y. Xianyu, Recent advances in gold nanoparticles-based biosensors for food safety detection, Biosens. Bioelectron. 179 (2021), 113076, https://doi.org/10.1016/j.bios.2021.113076.
[6] R. Moldovan, B.-C. Iacob, C. Farcău, E. Bodoki, R. Oprean, Strategies for SERS detection of organochlorine pesticides, Nanomaterials 11 (2021) 304, https://doi.org/10.3390/nano11020304.
[7] X. Xu, H. Yang, Q. Li, B. Yang, X. Wang, F.S.C. Lee, Residues of organochlorine pesticides in near shore waters of LaiZhou Bay and JiaoZhou Bay, Shandong Peninsula, China, Chemosphere 68 (2007) 126–139, https://doi.org/10.1016/j.chemosphere.2006.12.021.
[8] M. Ali, A.A. Kazmi, N. Ahmed, Study on effects of temperature, moisture and pH in degradation and degradation kinetics of aldrin, endosulfan, lindane pesticides during full-scale continuous rotary drum composting, Chemosphere 102 (2014) 68–75, https://doi.org/10.1016/j.chemosphere.2013.12.022.
[9] D. Guillén, A. Ginebreda, M. Farré, R.M. Darbra, M. Petrovic, M. Gros, D. Barceló, Prioritization of chemicals in the aquatic environment based on risk assessment: analytical, modeling and regulatory perspective, Sci. Total Environ. 440 (2012) 236–252, https://doi.org/10.1016/j.scitotenv.2012.06.064.
[10] T. Itoh, Y.S. Yamamoto, Between plasmonics and surface-enhanced resonant Raman spectroscopy: toward single-molecule strong coupling at a hotspot, Nanoscale 13 (2021) 1566–1580, https://doi.org/10.1039/d0nr07344j.

[11] J. Langer, D. Jimenez de Aberasturi, J. Aizpurua, R.A. Alvarez-Puebla, B. Auguié, J. J. Baumberg, G.C. Bazan, S. Bell, A. Boisen, A.G. Brolo, J. Choo, D. Cialla-May, V. Deckert, L. Fabris, K. Faulds, F.J. García de Abajo, R. Goodacre, D. Graham, A. J. Haes, C.L. Haynes, C. Huck, T. Itoh, M. Käll, J. Kneipp, N.A. Kotov, H. Kuang, E. C. Le Ru, H.K. Lee, J.F. Li, X.Y. Ling, S.A. Maier, T. Mayerhöfer, M. Moskovits, K. Murakoshi, J.M. Nam, S. Nie, Y. Ozaki, I. Pastoriza-Santos, J. Perez-Juste, J. Popp, A. Pucci, S. Reich, B. Ren, G.C. Schatz, T. Shegai, S. Schlücker, L.L. Tay, K. G. Thomas, Z.Q. Tian, R.P. Van Duyne, T. Vo-Dinh, Y. Wang, K.A. Willets, C. Xu, H. Xu, Y. Xu, Y.S. Yamamoto, B. Zhao, L.M. Liz-Marzán, Present and future of surface-enhanced Raman scattering, ACS Nano 14 (2020) 28–117, https://doi.org/10.1021/acsnano.9b04224.
[12] S.H. Yazdi, I.M. White, A nanoporous optofluidic microsystem for highly sensitive and repeatable surface enhanced Raman spectroscopy detection, Biomicrofluidics 6 (2012), 014105, https://doi.org/10.1063/1.3677369.
[13] W.W. Yu, I.M. White, Inkjet-printed paper-based SERS dipsticks and swabs for trace chemical detection, Analyst 138 (2013) 1020–1025, https://doi.org/10.1039/c2an36116g.
[14] W.W. Yu, I.M. White, A simple filter-based approach to surface enhanced Raman spectroscopy for trace chemical detection, Analyst 137 (2012), https://doi.org/10.1039/c2an15947c, 1168-73.
[15] Y. Nie, Y. Teng, P. Li, W. Liu, Q. Shi, Y. Zhang, Label-free aptamer-based sensor for specific detection of malathion residues by surface-enhanced Raman scattering, Spectrochim. Acta Part A Mol. Biomol. Spectrosc. 191 (2018) 271–276, https://doi.org/10.1016/j.saa.2017.10.030.
[16] F. Fathi, F. Lagugné-Labarthet, D.B. Pedersen, H.-B. Kraatz, Studies of the interaction of two organophosphonates with nanostructured silver surfaces, Analyst 137 (2012), https://doi.org/10.1039/c2an35641d, 4448-53.
[17] E. Dyguda-Kazimierowicz, S. Roszak, W.A. Sokalski, Alkaline hydrolysis of organophosphorus pesticides: the dependence of the reaction mechanism on the incoming group conformation, J. Phys. Chem. B 118 (2014) 7277–7289, https://doi.org/10.1021/jp503382j.
[18] W. Li, X. Yan, C. Gao, J. Duan, S. Beecham, A consecutive chlorination and alkaline hydrolysis process for rapid degradation and detoxication of malathion in aqueous solution, Chem. Eng. J. 392 (2020), 123793, https://doi.org/10.1016/j.cej.2019.123793.
[19] J. Yu, Y. Liu, S. Zhang, L. Luo, L. Zeng, Effect of brewing conditions on phytochemicals and sensory profiles of black tea infusions: a primary study on the effects of geraniol and β-ionone on taste perception of black tea infusions, Food Chem. 354 (2021), 129504, https://doi.org/10.1016/j.foodchem.2021.129504.
[20] B.N. Singh, Prateeksha, A.K.S. Rawat, R.M. Bhagat, B.R. Singh, Black tea: phytochemicals, cancer chemoprevention, and clinical studies, Crit. Rev. Food Sci. Nutr. 57 (2017) 1394–1410, https://doi.org/10.1080/10408398.2014.994700.
[21] S. Mao, C. Lu, M. Li, Y. Ye, X. Wei, H. Tong, Identification of key aromatic compounds in Congou black tea by partial least-square regression with variable importance of projection scores and gas chromatography-mass spectrometry/gas chromatography-olfactometry, J. Sci. Food Agric. 98 (2018) 5278–5286, https://doi.org/10.1002/jsfa.9066.
[22] X. Chen, Y. Xu, L. Meng, X. Chen, L. Yuan, Q. Cai, W. Shi, G. Huang, Non-parametric partial least squares–discriminant analysis model based on sum of ranking difference algorithm for tea grade identification using electronic tongue data, Sens. Actuators B Chem. 311 (2020), 127924, https://doi.org/10.1016/j.snb.2020.127924.
[23] L. Meng, X. Chen, X. Chen, L. Yuan, W. Shi, Q. Cai, G. Huang, Linear and nonlinear classification models for tea grade identification based on the elemental profile, Microchem. J. 153 (2020), 104512, https://doi.org/10.1016/j.microc.2019.104512.
[24] L.E. Eberly, Multiple linear regression, in: W.T. Ambrosius (Ed.), Topics in Biostatistics, Humana Press, Totowa, NJ, 2007, pp. 165–187, https://doi.org/10.1007/978-1-59745-530-5_9.
[25] A.D. Becke, Density-functional thermochemistry. III. The role of exact exchange, J. Chem. Phys. 98 (1993) 5648–5652, https://doi.org/10.1063/1.464913.
[26] A.D. Becke, Density-functional thermochemistry. IV. A new dynamical correlation functional and implications for exact-exchange mixing, J. Chem. Phys. 104 (1996) 1040–1046, https://doi.org/10.1063/1.470829.
[27] M.H. Jamróz, Vibrational energy distribution analysis (VEDA): scopes and limitations, Spectrochim. Acta Part A Mol. Biomol. Spectrosc. (2013) 220–230, https://doi.org/10.1016/j.saa.2013.05.096.
[28] T. Lu, F. Chen, Multiwfn: a multifunctional wavefunction analyzer, J. Comput. Chem. 33 (2012) 580–592, https://doi.org/10.1002/jcc.22885.
[29] F. Nie, L. Ga, J. Ai, One-pot synthesis of nucleoside-templated fluorescent silver nanoparticles and gold nanoparticles, ACS Omega 4 (2019) 7643–7649, https://doi.org/10.1021/acsomega.9b00701.
[30] P. Wulandari, T. Nagahiro, N. Fukada, Y. Kimura, M. Niwano, K. Tamada, Characterization of citrates on gold and silver nanoparticles, J. Colloid Interface Sci. 438 (2015) 244–248, https://doi.org/10.1016/j.jcis.2014.09.078.
[31] S.G. Balwe, V.V. Shinde, A.A. Rokade, S.S. Park, Y.T. Jeong, Green synthesis and characterization of silver nanoparticles (Ag NPs) from extract of plant Radix Puerariae: an efficient and recyclable catalyst for the construction of pyrimido[1,2-b]indazole derivatives under solvent-free conditions, Catal. Commun. 99 (2017) 121–126, https://doi.org/10.1016/j.catcom.2017.06.006.
[32] A.S. Hassanien, U.T. Khatoon, Synthesis and characterization of stable silver nanoparticles, Ag-NPs: discussion on the applications of Ag-NPs as antimicrobial agents, Phys. B Condens. Matter 554 (2019) 21–30, https://doi.org/10.1016/j.physb.2018.11.004.
[33] D.V. Leff, P.C. Ohara, J.R. Heath, W.M. Gelbart, Thermodynamic control of gold nanocrystal size – experiment and theory, J. Phys. Chem. 99 (1995) 7036–7041, https://doi.org/10.1021/j100018a041.
[34] J. Liu, R. Liu, Y. Yin, G. Jiang, Triton X-114 based cloud point extraction: a thermoreversible approach for separation/concentration and dispersion of nanomaterials in the aqueous phase, Chem. Commun. (2009) 1514–1516, https://doi.org/10.1039/B821124H.
[35] Q. Zhang, W. Li, C. Moran, J. Zeng, J. Chen, L.-P. Wen, Y. Xia, Seed-mediated synthesis of Ag nanocubes with controllable edge lengths in the range of 30−200 nm and comparison of their optical properties, J. Am. Chem. Soc. 132 (2010) 11372–11378, https://doi.org/10.1021/ja104931h.
[36] M. Mikołajczyk, B. Ziemnicka, J. Krzywański, M. Cypryk, B. Gostyński, Nucleophilic substitution at tetracoordinate phosphorus. Stereochemical course and mechanisms of nucleophilic displacement reactions at phosphorus in diastereomeric cis- and trans-2-Halogeno-4-methyl-1,3,2-dioxaphosphorinan-2-thiones: experimental and DFT, Molecules 26 (2021) 3655, https://doi.org/10.3390/molecules26123655.
[37] V.K. Balakrishnan, X. Han, G.W. VanLoon, J.M. Dust, J. Toullec, E. Buncel, Acceleration of nucleophilic attack on an organophosphorothioate neurotoxin, fenitrothion, by reactive counterion cationic micelles. Regioselectivity as a probe of substrate orientation within the micelle, Langmuir 20 (2004) 6586–6593, https://doi.org/10.1021/la049572d.
[38] E. Dyguda-Kazimierowicz, W.A. Sokalski, J. Leszczynski, Gas-Phase mechanisms of degradation of hazardous organophosphorus compounds: do they follow a common pattern of alkaline hydrolysis reaction as in phosphotriesterase? J. Phys. Chem. B 112 (2008) 9982–9991, https://doi.org/10.1021/jp800386f.
[39] V. López-Canut, M. Roca, J. Bertrán, V. Moliner, I. Tuñón, Theoretical study of phosphodiester hydrolysis in nucleotide pyrophosphatase/phosphodiesterase. Environmental effects on the reaction mechanism, J. Am. Chem. Soc. 132 (2010) 6955–6963, https://doi.org/10.1021/ja908391v.
[40] Zhao, L. Jensen, G.C. Schatz, Pyridine-Ag20 cluster: a model system for studying surface-enhanced Raman scattering, J. Am. Chem. Soc. 128 (2006) 2911–2919, https://doi.org/10.1021/ja0556326.
[41] A. Otto, J. Billmann, J. Eickmans, U. Ertürk, C. Pettenkofer, The "adatom model" of SERS (surface enhanced Raman scattering): the present status, Surf. Sci. 138 (1984) 319–338, https://doi.org/10.1016/0039-6028(84)90251-6.
[42] D.Y. Wu, M. Hayashi, S.H. Lin, Z.Q. Tian, Theoretical differential Raman scattering cross-sections of totally-symmetric vibrational modes of free pyridine and pyridine–metal cluster complexes, Spectrochim. Acta Part A Mol. Biomol. Spectrosc. 60 (2004) 137–146, https://doi.org/10.1016/S1386-1425(03)00190-2.
[43] R. Sun, W. Yang, Y. Li, C. Sun, Multi-residue analytical methods for pesticides in teas: a review, Eur. Food Res. Technol. 247 (2021) 1839–1858, https://doi.org/10.1007/s00217-021-03765-3.
[44] M. Anastassiades, S.J. Lehotay, D. Štajnbaher, F.J. Schenck, Fast and easy multiresidue method employing acetonitrile extraction/partitioning and "dispersive solid-phase extraction" for the determination of pesticide residues in produce, J. AOAC Int. 86 (2003) 412–431, https://doi.org/10.1093/jaoac/86.2.412.
[45] D.-Y. Wu, J.-F. Li, B. Ren, Z.-Q. Tian, Electrochemical surface-enhanced Raman spectroscopy of nanostructures, Chem. Soc. Rev. 37 (2008) 1025–1041, https://doi.org/10.1039/B707872M.
[46] E.C. Le Ru, E. Blackie, M. Meyer, P.G. Etchegoin, Surface enhanced Raman scattering enhancement factors: a comprehensive study, J. Phys. Chem. C 111 (2007) 13794–13803, https://doi.org/10.1021/jp0687908.
[47] A. Otto, I. Mrozek, H. Grabhorn, W. Akemann, Surface-enhanced Raman scattering, J. Phys. Condens. Matter 4 (1992) 1143–1212, https://doi.org/10.1088/0953-8984/4/5/001.

Xiaojing Chen received B.S, M.S, and Ph.D. degrees from Xiamen University, Third Institute of Oceanography State oceanic Administration and Xiamen University in 2001, 2005 and 2009, respectively. He worked at the college of Electrical and Electronic Information Engineering, Wenzhou University, Wenzhou, Zhejiang province, People's Republic of China, from June 2009. His main research interests focus on spectroscopy analysis, data mining, chemometrics, multivariate data analysis and food quality control.

Xixi Huang received her BE degree in Wenzhou University in 2019, and now she is a master student in college of electrical and electronic engineering, Wenzhou University. Her main research interests focus on rapid detection of food safety based on spectroscopy and sensor technology.

Shiliang Chen received B.S and M.S degrees from Fuzhou University in 2011 and 2015, respectively. He worked at Wenzhou University, Wenzhou, Zhejiang province, People's Republic of China. His main research interests focus on application of rapid detection based on SERS technology.